Aquaporin-9 is involved in the lipid-lowering activity of the nutraceutical silybin on hepatocytes through modulation of autophagy and lipid droplets composition

Francesca Baldini[1], Piero Portincasa[2], Elena Grasselli[1], Gianluca Damonte[3], Annalisa Salis[1], Michela Bonomo[4], Marilina Florio[4], Nadia Serale[1], Adriana Voci[1], Patrizia Gena[4], Laura Vergani[1,&,*] and Giuseppe Calamita[4,&,*]

[1]DISTAV, Dept. of Earth, Environment and Life Sciences; [2]Clinica Medica "A. Murri", Dept. of Biomedical Sciences and Human Oncology, Medical School, University of Bari "Aldo Moro", Italy; [3]Dept. of Experimental Medicine, University of Genova, Italy; [4]Dept. of Biosciences, Biotechnologies and Biopharmaceutics, University of Bari "Aldo Moro", Italy.

[&]Equally contributed

***To whom correspondence should be addressed:**
Giuseppe Calamita (giuseppe.calamita@uniba.it)
Laura Vergani (laura.vergani@unige.it)

Key words
Steatosis, steatohepatitis, silybin, aquaglyceroporins, hepatic glycerol, mono-unsaturated and saturated fatty acids, autophagy

List of abbreviations

AQP, aquaporin; Atg, autophagy-related proteins; COX, cytochrome c oxidase; FA, fatty acids FAME, fatty acid methyl ester; G3P, glycerol-3-phosphate; LC3: Atg8/MAP1LC3, microtubule associated protein 1 light-chain 3; LD, lipid droplets; miRNA, microRNAs; MUFA, monounsaturated fatty acid; NAFLD, non-alcoholic fatty liver disease; NASH, non-alcoholic steatohepatitis; NEFA, non-esterified fatty acid; OA, oleic acid; PA, palmitic acid; PCKS9, proprotein convertase subtilisin/kexin type 9; SCD-1, Stearoyl-CoA desaturase; SFA, saturated fatty acid; TG, triglycerides; UCP2, uncoupling protein 2; VLCAD, very long-chain acyl-CoA dehydrogenase; VLDL, very low density lipoproteins.

ABSTRACT

Hepatic steatosis is the hallmark of non-alcoholic fatty liver disease (NAFLD), the hepatic manifestation of the metabolic syndrome and insulin resistance with potential evolution towards non-alcoholic steatohepatitis (NASH), cirrhosis and hepatocellular carcinoma. Key roles of autophagy and oxidative stress in hepatic lipid accumulation and NAFLD progression are recognized. Here, we employed a rat hepatoma cell model of NAFLD progression made of FaO cells exposed to oleate/palmitate followed or not by TNFα treatment to investigate the molecular mechanisms through which silybin, a lipid-lowering nutraceutical, may improve hepatic lipid dyshomeostasis. The beneficial effect of silybin was found to involve amelioration of the fatty acids profile of lipid droplets, stimulation of the mitochondrial oxidation and upregulation of a microRNA of pivotal relevance in hepatic fat metabolism, miR-122. Silybin was also found to restore the levels of Aquaporin-9 (AQP9) and glycerol permeability while reducing the activation of the oxidative stress-dependent transcription factor NF-κB, and autophagy turnover. In conclusion, silybin was shown to have molecular effects on signaling pathways that were previously unknown and potentially protect the hepatocyte. These actions intersect TG metabolism, fat-induced autophagy and AQP9-mediated glycerol transport in hepatocytes.

1. INTRODUCTION

Non-alcoholic fatty liver disease (NAFLD) is accompanying the growing epidemics of obesity, type 2 diabetes, and metabolic syndrome worldwide (Krawczyk et al., 2010). In this context, hepatic steatosis is the response to high levels of fatty acids (FA) from diet and adipose tissue, as well as from intrahepatic *de novo* lipogenesis and defective export as very low density lipoproteins (VLDL) (Vergani, 2019). FA entering the hepatocytes are mainly esterified with glycerol to originate triglycerides (TG). The saturated palmitic acid (PA, 16:0) and the monounsaturated oleic acid (OA, 9-cis 18:1) are the most abundant FA in both diet and serum, and they show different lipotoxicity. In rodent hepatocytes cultured *in vitro*, excess PA induces apoptosis, whereas OA prevents cell death and promotes TG secretion (Ricchi et al., 2009). The formation of monounsaturated fatty acids (MUFAs) from saturated fatty acids (SFAs) is catalyzed mainly by the stearoyl-CoA desaturase (SCD-1) (Paton & Ntambi, 2009). In hepatocytes, TG are either packed as lipid droplets (LD) for storing, or as VLDL for secretion (Donnel et al., 2005).

The proprotein convertase subtilisin/kexin type 9 (PCSK9) is a hepatic protease that degrades the low-density lipoprotein receptor (LDLR) thereby elevating plasma LDL cholesterol levels (Lagace et al., 2006). Moreover, PCSK9 is involved in TG metabolism by acting on degradation of CD36, a major receptor involved in transport of long-chain FA and TG storage (Demers et al., 2015).

Although storing of lipids inside LD is beneficial, excess hepatocyte enlargement may result in cell dysfunction (Yamahguchi et al., 2007; Baldini et al., 2019), and benign hepatic steatosis can progress to non-alcoholic steatohepatitis (NASH), cirrhosis and hepatocellular carcinoma (Eckel et al., 2010). Adipokines, interleukins and Tumor Necrosis Factor α (TNFα) are known mediators of NAFLD progression (Bekaert et al., 2016). As a defense mechanism, excess TG accumulation promotes autophagy of LD (lipophagy) (Wang, 2016). Conventional autophagy is driven by a concerted action of a suite of "autophagy-related" molecules (Atg). The Atg8/MAP1LC3 (microtubule associated protein 1 light-chain 3, hereafter referred to as LC3) acts in elongation and maturation of the autophagosome, while Atg7 mediates the conversion of LC3-I to the active form LC3-II (Choi et al., 2013). Autophagy dysfunction has been linked to development of NAFLD (Kwanten et al., 2016).

The mobilization of lipids from LD results in excess FA entering oxidation pathways (Vergani, 2019). The long chain FA are oxidized mainly in mitochondria, where the very long-chain acyl-CoA dehydrogenase (VLCAD) catalyzes the first step of oxidation (Primassin et al., 2011), the cytochrome c oxidase (COX) in the respiratory chain converts molecular oxygen to water (Vecchione et al., 2017), and the uncoupling protein 2 (UCP2) in the inner membrane dissipates excess energy by separating oxidative phosphorylation from ATP synthesis (Baffy, 2005).

Stimulation of fat oxidation induces oxidative stress that promotes increased production of TNFα in adipose tissue and in the liver, which, in turn, may induce mitochondrial dysfunction. On the other hand, oxidative stress and stimulated autophagy activate the transcription factor NF-κB which regulates the expression of a broad range of anti-oxidants genes (Criollo et al., 2012), plays anti-apoptotic and pro-inflammatory functions and inhibits autophagy (Schlottmann et al., 2008).

MicroRNAs (miRNAs) are non-protein-coding, small single-stranded RNA, that bind to the 3′-UTR of the nucleotide sequence leading to inhibition of translation or mRNA degradation (Ambros, 2004). Dysregulation of miRNA expression has been observed in rodent models of NAFLD, often aligning with the changes observed in patients with steatosis and NASH (Cheung et al., 2008; Kong et al., 2011). In the liver, miR-122 represents about 70% of total miRNA and its down- or up-regulation can modify FA and cholesterol metabolism (Jin et al., 2014).

Aquaporin-9 (AQP9) belongs to *Aquaglyceroporins*, a branch of the *Aquaporin* family of membrane channels allowing permeation of glycerol and, to a lesser extent, water, hydrogen peroxide, urea and ammonia (Bernardino et al., 2016; Tesse et al., 2018). In liver, AQP9 represents the major route through which hepatocytes import glycerol (Jelen et al, 2011; Calamita et al., 2012; Calamita et al., 2015; Gena et al., 2017). Reduction in hepatic AQP9 levels resulting in reduced glycerol permeability decreases substrate availability for the TG synthesis in the cell (Portincasa et al., 2008; Calamita et al., 2015). Hepatic AQP9 is regulated by insulin and leptin (Rodriguez et al., 2011), and its pathophysiological relevance was shown in both cell and animal models of NAFLD, and in liver biopsies of obese patients with NAFLD (Gena et al., 2013; Rodriguez et al., 2014; Rodriguez et al., 2015a; Rodriguez et al., 2015b). Male rats fed a high-fat diet (HFD) show reduction in liver steatosis after knock-down of liver *Aqp9* at disease onset (Cai et al., 2013). Leptin-deficient mice, an animal model of NAFLD, have decreased levels of hepatic AQP9 (Gena et al., 2013). Therefore, AQP9 might become an additional therapeutic target for treatment of NAFLD/NASH (Calamita & Portincasa, 2007; Calamita et al., 2018). The possible correlation between AQP9 and autophagy in hepatic lipid metabolism needs to be investigated (Kwanten et al., 2016), as changes in AQP9 may prevent or reduce TG accumulation through autophagy (Calamita et al., 2018).

So far, therapeutic options in NAFLD and NASH are lacking, and currently the best approach is limited to changes of lifestyles (i.e. balanced diet, regular physical exercise, and reduction of overweight) (Molina-Molina et al., 2018). As oxidative stress seems to have a central role in hepatic cell injury in the context of NASH, the influence of several antioxidants such as the phytochemical silybin and other compounds are being actively investigated. Silybin is the most relevant flavonolignan of silymarin, the extract of milk thistle seed (*Silybum marianum)*. Silybin has

antioxidant, anti-inflammatory and cytoprotective actions and it has been used in patients with NAFLD with some beneficial effects (Loguercio & Festi, 2011; Loguercio et al., 2012). Here, in addition to a significant amelioration of the lipid profile of LD, we report involvement of AQP9 in the lipid-lowering activity of silybin on a hepatocyte model of NAFLD through modulation of autophagy.

2. MATERIALS AND METHODS

2.1 Chemicals

All chemicals, unless otherwise indicated, were supplied by Sigma-Aldrich Corp. (Milan, Italy).

2.2 Cell Treatments

Rat hepatoma FaO cells [The European Collection of Authenticated Cell Cultures (ECACC)], (Clayton et al., 1985) were grown in Coon's modified Ham's F12 with 10% foetal bovine serum (FBS). Cells grown until 80% confluence were incubated in high-glucose medium with 0.25% bovine serum albumin (BSA) to increase stability and solubility of FA (Vergani et al., 2018). A condition mimicking human steatosis (SS) was induced by incubating FaO cells for 3 h with an oleate/palmitate mixture (2:1 molar ratio, final concentration 0.75 mM). A steatohepatitis (SH) condition was mimicked by incubating SS cells for 24 h with 10 ng/mL TNFα (Zhang et al., 2010). After replacing the medium, both SS and SH cells were treated for 24 h with 50 μM silybin (Sil) (Istituto Biochimico Italiano, Lorenzini SpA, Italy) (Vecchione et al., 2016). Silybin stock (10 mM) was prepared in dimethyl sulfoxide (DMSO).

2.3 Lipid Droplet imaging

Cells grown on coverslips were rinsed with PBS and neutral lipids were visualized by optical microscopy using the selective Oil-Red-O (ORO) dye (Koopman et al., 2001). Briefly, after fixing in 4% paraformaldehyde for 20 min at room temperature, cells were washed with PBS, stained for 30 min with 0.3% ORO solution in isopropanol 60%. After fixation and washing, cells were mounted with 4′,6-diamidino-2-phenylindole (DAPI). Images were obtained using a Leica DMRB light microscope equipped with a Leica CCD camera DFC420C (Leica, Wetzlar, Germany). A first image was obtained by acquiring the ORO-stained LD with bright field set-up, then a second image of the DAPI stained nuclei was acquired with fluorescence set-up. Images were captured with 40x objective and merged (Khalil et al., 2019). Both the average size and the number of LD/cell were evaluated on acquired images using the open source image processing program ImageJ free software (http://imagej.nih.gov/ij/). At least five images from random fields in each sample were

acquired for each experiment set, and at least forty cells for each image were analyzed. Values were expressed as mean ± S.D. from at least three independent experiments.

2.4 Lipid Droplet isolation and composition

Lipid droplets were isolated from cells following a standard protocol with minor modifications (Atshaves et al., 2001). FaO cells were scraped from the dishes. Cell suspension (about $40x10^6$ cells/sample) was homogenized with a glass dounce homogenizer on ice, and centrifuged at 800xg for 10 min at 4 °C. The supernatant was centrifuged at 5,000xg for 20 min. Then the supernatant was further centrifuged at 43,000 rpm in SW55 rotor (230,000xg) for 2 h at 4 °C. The LD fraction forming a distinct white band on the surface of the preparation was collected. Lipids were then extracted from isolated LD using the method of Folch et al. (Folch et al., 1957) as previously described (Grasselli et al., 2014). Briefly, the lipid phase was saponified with methanolic KOH (3 M) and the non-saponifiable lipids were extracted by diethylether, and the aqueous phase was acidified and extracted with n-hexane. The hexane phases containing NEFAs were collected, the solvent evaporated, and the residue derivatized by acid-catalyzed esterification (Morrison & Smith, 1964). Then, samples resuspended in hexane were injected in a HP5890 series II gas chromatograph coupled to a HP5970 mass spectrometer equipped with an electron impact ionization source (Agilent). Separation was performed on a DB5MS capillary column (Phenomenex, 0.25 mm × 30 m); the helium gas flow was 1 mL/min. The oven temperature gradient was as follows: initial temperature of 100 °C, isothermal at 100 °C for 3 min, 100 to 300 °C (rate, 15 °C/min) and isothermal at 300 °C for 5 min. The MS analysis was performed in full-scan mode. FAME (fatty acid methyl ester) quantification was performed using a calibration curve obtained injecting different FAME standards referring to selected ions. The most abundant and specific ions were used for the quantification of FAMEs: m/z 74 was used for saturated FAMEs and m/z 55 for monosaturated FAMEs. The regression curves were linear in the range of the FAME concentrations used for the analysis.

2.5 RNA extraction and real-time qPCR

RNA was isolated using Trizol reagent, cDNA was synthesized and quantitative real-time PCR (qPCR) performed in quadruplicate using 1x IQ™SybrGreen SuperMix and Chromo4™ System apparatus (Biorad, Milan, Italy) as previously described (Grasselli et al., 2016). The relative quantity of target mRNA was calculated by the comparative Cq method using glyceraldehyde 3-phosphate dehydrogenase (GAPDH) as housekeeping gene, and expressed as fold induction with respect to controls (Vecchione et al., 2016). Primer pairs designed *ad hoc* starting from the coding

sequences of *Rattus norvegicus* (http://www.ncbi.nlm.nih.gov/Genbank/GenbankSearch.html) and synthesized by TibMolBiol (Genova, Italy) are listed in Table 1.

Expression of miRNA 122 (miR-122) was measured as described elsewhere (Baselga-Escudero et al., 2015). Briefly, reverse transcription was performed using the High capacity cDNA kit (ThermoFisher Scientific, Milan, Italy), following manufacturer's instructions, and the miRNA-specific reverse-transcription primers provided with the TaqMan MicroRNA Assay (ThermoFisher Scientific, Milan, Italy). Amplification was performed using the Stepone plus Real-Time PCR system (ThermoFisher Scientific) at 50 °C for 2 min and at 95 °C for 10 min followed by 40 cycles at 95 °C for 15 s and 60 °C for 1 min. Probe and primers for both miRNA-122-5p (4427975-002245) and miRNA U6 (4427975-001973) were purchased from ThermoFisher Scientific. The relative quantity of miRNA-122-5p was calculated by the comparative Cq method using miRNA U6 as housekeeping gene and expressed as fold induction with respect to controls.

2.6 Immunofluorescence of LC3 and AQP9

Cells grown on poly-L-lysine coated coverslips were rinsed with phosphate-buffered saline (PBS) at pH 7.4, fixed with 4% paraformaldehyde for 20 min and then permeabilized with 0.1% Triton X-100 for 15 min at room temperature (RT). After several washings (3 times for 5 min), slides were blocked with 0.1% gelatin in PBS for 15 min and incubated for 2 h at RT with rabbit polyclonal anti-LC3 (14600-1-AP; Proteintech, Manchester, UK) and/or anti-AQP9 affinity-purified antibodies (AQP9-1A; Alpha Diagnostics International, San Antonio, TX) at a concentration of 3 μg/mL and 4 μg/mL, respectively, in blocking solution (PBS added with 0.1% gelatin). Successively, slides were washed and incubated with fluorescein-isothiocyanate (FITC)-conjugated secondary antibody (Alexa Fluor 488; Thermo Fisher Scientific, Milano, Italy) diluted 1:1000 in blocking solution for 1 h at RT. After staining, slides were washed thoroughly with PBS and mounted with an anti-fade medium containing DAPI (Vectashield, DBA, Segrate, Italy). Finally, slides were sealed and viewed with a Nikon Eclipse 600 photomicroscope equipped with a Nikon DMX 1200 camera (Nikon Instruments SpA, Calenzano, Italy).

2.7 Cytochrome C oxidase activity

Cytochrome C oxidase (COX) is the terminal enzyme complex in the respiratory chain. COX activity was assayed according to Moyes and coworkers (Moyes et al., 1997) following the decrease in absorbance at 550 nm. Briefly, 50 μM reduced cytochrome c was dissolved in 0.5% Tween-20 in 20 mM Tris-HCl (pH 8.0). Cytochrome c was reduced with ascorbate and dialyzed overnight to remove unreacted ascorbate. Then, the concentration of reduced cytochrome c was determined

using an ε_{550}=28.5 mM^{-1}. Immediately before the assay, cell extracts (about 3–10×10^4 cells) were added to the assay medium and incubated for 5 min. The reaction was started by adding 10 μM reduced cytochrome c and the change in absorbance was recorded at 550 nm for 3 min.

2.8 Western blotting

Immunoblotting analyses to assess the protein level of LC3α/β and of NF-kB were performed as previously described (Vecchione et al., 2017). For LC3α/β immunoblotting cells were lysed on ice in lysis buffer (NaCl 150 mM, Tris HCl pH 7.4, 50 mM, SDS 0.33%). For of NF-kB, nuclei were isolated by suspending the cellular pellet in 400 μL ice-cold Buffer A (20 mM Tris-HCl pH 7.8, 50 mM KCl, 10 μg/mL Leupeptin, 0.1 mM Dithiothreitol-DTT, 1 mM phenylmethanesulfonyl fluoride-PMSF); and 400 μL Buffer B (Buffer A plus 1.2% Nonindet P40). The suspension was vortex-mixed for 10 s, centrifuged, and washed. The nuclear pellet was resuspended in 100 μL Buffer B, mixed thoroughly in ice for 15 min and finally centrifuged. The supernatant containing the nuclear extracts was collected. About 30-50 μg proteins were electrophoresed on 10% sodium dodecyl sulfate polyacrylamide gel electrophoresis (SDS-PAGE) (Laemmli, 1970). Membrane was blocked in 5% fat-free milk/PBST (pH 7.4) and probed overnight at 4 °C using rabbit NF-kB p65 antibody (SC-109; Santa Cruz Biotechnology, DBA, Milan, Italy), or mouse anti-MAP LC3α/β p (SC-398822 Santa Cruz Biotechnology) in PBST buffer (PBS with 0.1% Tween 20) at 4°C (Towbin et al., 1979). Membranes were washed and incubated with horseradish peroxidase (HRP)-conjugated secondary antibody in PBST for 1 h at room temperature. Immune complexes were visualized using an enhanced chemiluminescence Western blotting analysis system (Bio-Rad ChemiDoc XRS System). Films were digitized and band optical densities were quantified against the actin band using a computerized imaging system and expressed as Relative Optical Density (ROD, arbitrary units). ROD of each band was expressed as percentage respect to control and about 30-50 μg proteins of cellular homogenates were electrophoresed on SDS polyacrylamide gel electrophoresis (SDS-PAGE).

2.9 Measurement of extracellular glycerol

Glycerol content was measured in cellular medium after a brief centrifugation (14,000xg for 3 min at 4°C) after separation in chloroform:methanol (2:1). The water-soluble glycerol was determined by using the 'Triglycerides liquid' kit (Sentinel, Milan, Italy) (Vecchone et al., 2016). Varian Cary 50 spectrophotometer (Agilent, Milan, Italy) was used for spectrophotometric analysis. Data were expressed as percent glycerol content relative to controls.

Statistical analysis

Data were expressed as means ± standard deviation (S.D.) of at least three independent experiments in triplicate. Statistical analysis was performed using ANOVA with Tukey's post-hoc test (GraphPad Software, Inc., San Diego, CA, USA).

3. RESULTS

3.1 Effect of silybin on the fatty acid composition of LD

The cytosolic accumulation of TG in the different steatotic conditions, as visualized by ORO staining, was associated with a marked increase in LD number and size compared to control cells (Fig. 1A-C). Control FaO cells showed only few (about 72 LD/cell) and small (about 0.9 μm average diameter) LD, while both number and size of LD resulted significantly increased in SS and SH cells. While the number of LD was comparable between SS and SH cells (about 295 LD/cell), the average size of LD in SH was smaller than in SS cells (1.3 μm *vs* 1.5 μm, respectively). In SS cells silybin reduced the LD diameter to a value similar to that of control cells (1.1 μm), without effects on the number of LD. No change in LD diameter was seen in the SH cells exposed to silybin.

Gas chromatography analysis of LD purified from steatotic cells (Fig. 2A) revealed an acyl composition of the TG in LD consistent with that typically found in mammalian cells in terms of both saturated (SFA) and unsaturated (UFA) fatty acids. The most abundant fatty acids stored in LD included SFA such as myristic acid (MA, 14:0), palmitic acid (PA, 16:0), stearic acid (SA, 18:0), and UFA such as oleic acid (OA, 18:1) and linoleic acid (LA, 18:2). Analytically, the acyl profile in LD from SS cells showed a prevalence of PA (50.1%), followed by SA (27.4%), OA (10.8%), MA (7.4%) and LA (4.2%). SH cells exhibited an increase in PA content (65.6%) and a decrease in OA (6.4%), MA (1.1%) and LA (0.6%) contents, while SA did not change (26.2%). Silybin did not markedly modify the FA pattern in SS cells whereas in SH cells led to a reduction in PA (to 46.5%) and SA (to 20.2%) content and to an increase in OA (to 11.5%) and MA (to 13.8%) levels.

Of note, SH cells showed a marked increase in SFA/UFA ratio compared to SS cells (13.7 *vs* 5.7 in SH and SS cells, respectively), and a reduction in the content of short-medium chain FA (<C16) (4.3% *vs* 11.6% in SS and SH cells, respectively) (Fig. 2A, panel). Treatment with silybin rescued the altered FA profile since the SFA/UFA ratio decreased when SH cells were treated with silybin (from 13.6 to 7.0% in SH and SH+Sil cells). On the other hand, treatment with silybin increased the amount of FA <C16 that reached mean values of 15.9% and 18.6% in SS+Sil and SH+Sil conditions, respectively.

~~This modulation of FA profile could be sustained by changes in SCD-1 mRNA expression~~. As shown in Figure 2B, both SS and SH cells showed a decrease in SCD-1 mRNA expression compared to control (0.39- and 0.62-fold induction, respectively; $p \leq 0.01$ and $p \leq 0.05$, respectively), while treatment with silybin increased SCD-1 mRNA level of +249% ($p \leq 0.05$) and +292% ($p \leq 0.001$) with respect to their counterpart SS and SH, respectively.

3.2 Effect of silybin on hepatocyte AQP9, glycerol uptake and autophagy of LD

Since liver steatosis *in vivo* has been reported to lead to AQP9 dysregulation (Gena et al., 2013; Cai et al., 2013; Rodriguez et al., 2014) and dysfunctional autophagy (Kwanten et al., 2016) we assessed the possible changes in AQP9 expression, glycerol import and autophagic process in FaO cells in the different experimental conditions.

By real-time qPCR, no differences in *AQP9* transcript levels occurred in both steatotic SS and SH cells compared to control (Fig. 3A), whereas marked upregulation of AQP9 was observed in SS and SH cells exposed to silybin (1.55- and 1.72-fold induction *vs* control cells, in SS and SH cells, respectively; $p \leq 0.001$) (Fig. 3A). In terms of protein, SS and SH cells showed a significant reduction of plasma membrane AQP9 immunoreactivity compared to control cells (Fig. 3B,C,E), and silybin restored the levels of AQP9 protein in SS and SH cells (Fig. 3D,F) to extents comparable to those of the control FaO cells. No changes in the transcript and protein levels of AQP9 were seen in control cells receiving silybin (data not shown).

Given the role of AQP9 in glycerol transport within hepatocytes, we measured the glycerol concentration in the culture medium in the attempt of correlating the levels of AQP9 with those of the glycerol influx. The extracellular level of glycerol for both SS and SH cells was similar to that of control cells, while it was significantly reduced by the treatment with silybin (-41% for SS+Sil *vs* SS; –46% for SH+Sil *vs*. SH; $p \leq 0.001$) (Fig. 3G). ~~This suggests that silybin also acts by increasing the glycerol uptake through the augmentation of the AQP9 levels at the plasma membrane.~~

The possible effects of silybin on cell autophagy were investigated by assessing the intracellular expression and distribution of LC3-II, and by quantifying the LC3-II/LC3-I ratio (Tanida et al., 2004). In control conditions, only few punctuate structures, seen as green dots, were observed indicating LC3 recruitment on autophagosomes (Fig. 4A). Both SS and SH hepatocytes showed an increase in these cytosolic puncta (Fig. 4B, D), a profile indicating increased autophagy turnover accompanying NAFLD progression. The immunofluorescence was of wider diffusion when SS and SH were treated with silybin (Fig. 4C,E), resulting in a pattern more similar to that of the control cells (Fig. 4A). In line with these results, Western blot analysis (Fig. 4F) showed a significant

increase in LC3-II/LC3-I ratio in both SS and SH cells (+24% and +17%, respectively, *vs* control; $p \leq 0.001$ and $p \leq 0.05$), while silybin counteracted this increase in both steatotic conditions (−29% and -31%, respectively, *vs* their counterparts; $p \leq 0.001$). No changes in LC3-II/LC3-I ratio were seen in control FaO cells receiving silybin (data not shown).

~~The autophagosome formation is also regulated by Atg7 (Komatsu et al., 2005).~~ In both steatotic conditions the Atg7 mRNA was overexpressed, but the increase was larger in SH cells compared to SS cells (2.84 vs 1.53-fold induction *vs* control, respectively; $p \leq 0.01$ and $p \leq 0.001$) (Fig. 4G). On the other hand, silybin was able to restore Atg7 expression near to control in SH hepatocytes (-60% *vs* SH; $p \leq 0.001$).

Since autophagy is known to activate NF-κB we assessed by immunoblotting the NF-κB activation as a downstream effect of autophagy stimulation (Fig. 4H). A significant decrease in NF-κB activation was seen when both SS and SH hepatocytes were treated with silybin (about -30% for both SS and SH; $p \leq 0.05$).

3.3 Effects of silybin on genes of hepatic lipid metabolism

Uptake of circulating FA by hepatocytes is also regulated by PCSK9. Analysis by qPCR showed that *PCSK9* mRNA expression was downregulated in both SS and SH cells, with respect to control (0.59- and 0.45-fold induction, respectively; $p \leq 0.001$), and silybin partially reversed this downregulation as *PCSK9* mRNA expression increased significantly in SH cells (+102% *vs* SH; $p \leq 0.01$) (Fig. 5A). ~~Of note, a reduction in PCSK9 levels promoting the FA entry into hepatocytes may be a response to increased level of external FA.~~

Mitochondria are the final destination of long chain FA for β-oxidation. In mitochondria, expression of VLCAD (Fig. 5B), the shuttle for FA, was up-regulated in SS and SH cells with respect to control (1.61- and 1.86-fold induction, respectively; $p \leq 0.05$), and it was further stimulated when cells were treated with silybin (2.21- and 4.47-fold induction *vs* control, respectively; $p \leq 0.01$). COX acting in the mitochondrial electron transport chain (Fig. 5D) increased significantly its activity only in SH cells (+97% *vs* control; $p \leq 0.001$), but not in SS cells, and silybin was able to stimulate COX activity in SS cells (+27% *vs* control), but not in SH cells (Fig. 5C). Expression of the uncoupling protein UCP2 (Fig. 5D) was also up-regulated in SS and SH cells with respect to control (1.72- and 2.97-fold induction *vs* control; $p \leq 0.01$ and $p \leq 0.0011$, respectively), and silybin counteracted this upregulation (-31% with respect to SH cells; $p \leq 0.01$). Silybin did not play any significant effect on the expression/activity of these proteins in control FaO cells (data not shown).

In hepatocytes miR-122 is recognised to be a major regulator of lipid metabolism (Tsai et al., 2009). A significant increase in miR-122 level was observed in SS cells upon treatment with silybin (2.01-fold induction *vs* control; $p \leq 0.001$) (Fig. 5E).

4. DISCUSSION

NAFLD is a worrisome health problem worldwide commonly encountered with the metabolic syndrome. No established therapy exists for NAFLD, and changes in lifestyles remain the most common approaches to treat overweight, obesity, insulin resistance, and liver steatosis. The nutraceutical silybin has shown beneficial effects in patients with NAFLD (Loguercio et al., 2012), and potential hepatoprotective effects in both animal and cellular models of NAFLD (Grasselli et al., 2019; Vecchione et al., 2017; Vecchione et al., 2016; Grattagliano et al., 2013).

In the present study, employing a cellular model of NAFLD progression widely employed in previous studies (Baldini et al., 2019), we found that the beneficial effect of silybin on hepatic steatosis involves amelioration of the FA profile of LD, stimulation of the mitochondrial oxidation and upregulation of miR-122 expression. Interestingly, silybin is also found to restore the levels of AQP9 and glycerol permeability while reducing the autophagy triggered by the ectopic accumulation of lipids. These results suggest a rather complex and pleiotropic role for silybin in the hepatic cells, involving several key molecular intracellular pathways active during liver steatosis.

The accuracy of the cellular model of NAFLD progression was verified by a series of morphometric and biochemical parameters. First of all, steatotic FaO cells showed an increase in number/size of LD compared to controls. However, the LD diameter was smaller in SH cells than in SS cells, suggesting that these conditions mimic microvesicular and macrovesicular steatosis, respectively. Of note, differences in type of histological steatosis might correlate with distinct phenotypic and prognostic manifestations of liver steatosis. For example, in drug-induced liver injury, acute steatosis is severe, and usually microvesicular because of disrupted mitochondrial beta-oxidation of lipids and oxidative energy production (Cullen, 2005). Also, acute liver failure of pregnancy occurs as microvesicular steatosis (Bacq, 1998). More chronic forms of liver damage, by contrast, occur with macrovesicular steatosis as (Ramachandran and Kakar, 2009). However, treatment with silybin was able to reduce the number of LD in both SS and SH cells and the diameter of LD in SS cells, while did not play detectable effects on the size of LD in SH cells. Another sign that silybin improves hepatic steatosis is the increase in miR-122 level in SS cells upon treatment with silybin according to previous studies showing the involvement of miR-122 in NAFLD (Tsai et al., 2009). Indeed, *in vitro* studies showed downregulation of miR-122 in fatty hepatocytes, and reduced

expression of major lipogenic genes upon upregulation of miR-122 in HepG2 cells (Cheung et al., 2008).

In terms of acyl composition, the LD of SS cells are rich in the saturated fatty acids PA and SA, and of the unsaturated OA. The PA content increases in SH cells (+15% *vs* SS cells) being partially balanced by a reduction in OA content (-4% *vs* SS cells). SH cells showed also a lower content of short-medium chain FA (<C16) compared to SS cells. The changes in SFA/UFA ratio might be a sign of more severe steatosis in SH cells compared to SS cells. Of note, the beneficial effect of silybin in SH cells was accompanied to a reduction in content of the saturated fatty acids PA and SA, and to an increase in content of the unsaturated OA, as well as to an increase in the amount of short-medium chain FA. In both SS and SH cells, the changes in the FA profile of LDs could be sustained by downregulation of the *SCD-1* mRNA expression. Interestingly, silybin was able to counteract the SCD-1 mRNA downregulation.

Uptake of FA by hepatocytes is regulated by PCSK9, and this effect is independent of its action on LDLR (Demers et al., 2015). Indeed, PCSK9 binds LDLR resulting in its internalization and degradation (Horton et al., 2009), but PCSK9 promotes also degradation of CD36, which is involved in FA uptake and TG storage/secretion. Indeed, *Pcsk9*$^{-/-}$ mice develop hepatic steatosis with liver sections showing accumulation of LD and marked increase in TG content (Demers et al., 2015). In the present experimental steatogenic setting, *PCSK9* mRNA was downregulated in both SS and SH cells. This condition would likely promote FA entry in hepatocytes, a mechanism potentially counteracting the excess of external FA. Notably, silybin significantly reversed *PCSK9* downregulation in SH cells, and apparently restored cellular function while reducing FA influx in the hepatocyte. The potential "double sword" effect of PCSK9 inhibition/activation in the hepatocyte, and the action of silybin, needs to be shortly commented, due to potential effects on systemic lipid metabolism. *In vivo* dysfunctional PCSK9 leads to persistently elevated serum LDL-cholesterol and increased risk of coronary heart disease (Lagace et al., 2006), nevertheless loss-of-function mutations are frequently associated with decreased LDL-cholesterol and low risk of heart disease (Cohen et al., 2006, Benn et al., 2010). Of note, statins, acting as hypolipemic drugs, lead to increased levels of PCSK9 resulting in a LDL-C-lowering effect *in vitro* (Dubuc et al., 2004), but clinical studies do not confirm this effect (Huijgen et al., 2012). In this study, it appears that liver steatosis leads to dysregulation of PCSK9 (and possibly LDLR), while silybin restores at least in part the hepatocyte function. Furthermore, silymarin (and its main constituent silybin) are deemed as adjuvants in hyperlipoproteinemia (Skottova and Krecman, 1998) and reduce LDL lipid peroxidation. Silybin exerts an inhibitory effect on HMG-CoA reductase *in vitro* while, *in vivo*, reducing cholesterol synthesis (Cicero et al., 2017).

Together with the effect on other biomarkers of cardiovascular risk, the net effect of silymarin appears to be rather protective on the liver and on serum lipids (Voroneanu et al., 2016), although further studies need to investigate *in vivo* the effect of silybin on PCSK9-mediated effects during ongoing liver steatosis.

Mitochondria are the final destination of long chain FA for β-oxidation. In both SS and SH cells, UCP2 expression was upregulated in the attempt to avoid the excess synthesis of ATP. Moreover, as a response of toxic TG accumulation, SH cells stimulated the COX activity in the respiratory chain. The lipid lowering activity of silybin in both SS and SH cells was associated to increased long chain FA entering mitochondria through up-regulation of VLCAD expression.

Our results suggest that the anti-steatotic action of silybin implies upregulation of AQP9 and increase of glycerol permeability in hepatocytes. This result is an important insight into the full understanding of the role played by this aquaglyceroporin in NAFLD/NASH. In humans, AQP9 is highly expressed in liver (Lindskog et al, 2016), where in post-prandial conditions it sustains the hepatic import of extracellular glycerol for the *ex-novo* synthesis of TG. Likely, silybin might increase the AQP9 levels through an epigenetic mechanism as most bioactive plant polyphenols do (Joven et al, 2014).

Moreover, silybin is found to diminish the fat-stimulated autophagy as demonstrated by the downregulation of the LC3-II and Atg7 expression in both SS and SH hepatocytes. Indeed, the autophagosome formation is regulated by Atg7 (Komatsu et al., 2005). The parallel reduction in NF-κB activation upon treatment with this phytocompound well fits with the role of NF-κB activation in promoting autophagic process **(**Trocoli and Djavaheri-Mergny, 2011**)**.

The inverse correlation found between AQP9 levels and autophagy is compelling. Low levels of hepatocyte AQP9 were associated with the increased autophagy accompanying the TG overaccumulation, whereas the opposite was observed after restoring the levels of AQP9. This finding is consistent with hepatocyte AQP9 expression being positively regulated by the mammalian target of rapamycin (mTOR) (Rodriguez et al, 2011), a paramount signaling pathway in the regulation of autophagy as the initiation of autophagosome formation by phosphorylating UNC51-like kinase 1 (ULK1) is inhibited by mTOR (Ravikumar et al., 2009; Rubinsztein et al., 2012). Of note, AQP9 might have good potentials as drug target in preventing or treating NAFLD/NASH (Calamita et al., 2018), and small compounds selectively and potently gating the AQP9 channel are already available (Jelen et al., 2011; Wacker et al., 2013; Sonntag et al., 2019). The present results lead to the attractive idea that pharmacological modulation of AQP9 may prevent or reduce TG over accumulation and consequent liver dysfunction through autophagy.

In summary, the beneficial effect of silybin on the *in vitro* model of NAFLD and NASH implies (*i*) amelioration of the profile of FA stored in LD with an increase the short/medium chain FA ratio and a decrease of the saturated/monounsaturated FA ratio, (*ii*) stimulation of mitochondrial FA oxidation through upregulation of VLCAD and UCP2 and stimulation of COX activity, (*iii*) increase of the master regulator of hepatic lipid metabolism miR-122, (*iv*) increase of AQP9 expression and glycerol permeability, and (*iv*) diminution of fat-stimulated autophagy.

Altogether, these results show that silybin has molecular effects on signaling pathways that were previously unknown and potentially protect the hepatocyte. These effects intersect TG metabolism, fat-induced autophagy and AQP9-mediated glycerol transport in hepatocytes.

ACKNOWLEDGMENTS

We would like to thank Drs Rita Fabbri and Mohamad Khalil for the help with the experiments. Financial support to GC from Italian “Programmi di Ricerca Scientifica di Rilevante Interesse Nazionale 2017” (PRIN2017; grant # 2017J92TM5) and to LV from University of Genova are gratefully acknowledged.

DECLARATION OF COMPETING INTEREST

The authors declare they have no conflict of interest.

REFERENCES

- Krawczyk M, Bonfrate L, Portincasa P. Nonalcoholic fatty liver disease. Best Pract Res Clin Gastroenterol. 2010 Oct;24(5):695-708. doi: 10.1016/j.bpg.2010.08.005.
- Vergani L. Fatty acids and effects on in vitro and in vivo models of liver steatosis. Curr Med Chem. 2019;26(19):3439-3456. doi: 10.2174/0929867324666170518101334.
- Ricchi M, Odoardi MR, Carulli L, Anzivino C, Ballestri S, Pinetti A, Fantoni LI, Marra F, Bertolotti M, Banni S, Lonardo A, Carulli N, Loria P. Differential effect of oleic and palmitic acid on lipid accumulation and apoptosis in cultured hepatocytes. J Gastroenterol Hepatol. 2009 May;24(5):830-40. doi: 10.1111/j.1440-1746.2008.05733.x.
- Paton CM, Ntambi JM. Biochemical and physiological function of stearoyl-CoA desaturase. American Journal of Physiology. Endocrinology and Metabolism. 297 (1). PMID 19066317 Am J Physiol Endocrinol Metab. 2009 Jul;297(1):E28-37. doi: 10.1152/ajpendo.90897.2008.
- Donnelly KL, Smith CI, Schwarzenberg SJ, Jessurun J, Boldt MD, Parks EJ. Sources of fatty acids stored in liver and secreted via lipoproteins in patients with nonalcoholic fatty liver disease. The Journal of clinical investigation 2005; 115(5): 1343-51. doi:10.1172/JCI23621
- Lagace TA, Curtis DE, Garuti R, McNutt MC, Park SW, Prather HB, Anderson NN, Ho YK, Hammer RE, Horton JD. Secreted PCSK9 decreases the number of LDL receptors in hepatocytes and in livers of parabiotic mice. J Clin Invest. 2006 Nov;116(11):2995-3005. doi:10.1172/JCI29383
- Demers A, Samami S, Lauzier B, Des Rosiers C, Ngo Sock ET, Ong H, Mayer G. PCSK9 Induces CD36 Degradation and Affects Long-Chain Fatty Acid Uptake and Triglyceride Metabolism in Adipocytes and in Mouse Liver. Arterioscler Thromb Vasc Biol. 2015 Dec;35(12):2517-25. doi: 10.1161/ATVBAHA.115.306032.
- Yamaguchi K, Yang L, McCall S, Huang J, Yu XX, Pandey SK, Bhanot S, Monia BP, Li YX, Diehl AM. Inhibiting triglyceride synthesis improves hepatic steatosis but exacerbates liver damage and fibrosis in obese mice with nonalcoholic steatohepatitis. Hepatology 2007; 45(6): 1366-74. doi:10.1002/hep.21655.
- Baldini F, Bartolozzi A, Ardito M, Voci A, Portincasa P, Vassalli M, Vergani L. Biomechanics of cultured hepatic cells during different steatogenic hits. J Mech Behav Biomed Mater. 2019 Sep;97:296-305. doi: 10.1016/j.jmbbm.2019.05.036.
- Eckel RH, Alberti KG, Grundy SM, Zimmet PZ. The metabolic syndrome. Lancet 2010; 375(9710): 181-3. doi:10.1016/S0140-6736(09)61794-3.

- Bekaert M, Verhelst X, Geerts A, Lapauw B, Calders P. Association of recently described adipokines with liver histology in biopsy-proven non-alcoholic fatty liver disease: a systematic review. Obese Rev. 2016 Jan;17(1):68-80. doi: 10.1111/obr.12333.
- Wang CW. Lipid droplets, lipophagy, and beyond. Biochim Biophys Acta. 2016 Aug;1861(8 Pt B):793-805. doi: 10.1016/j.bbalip.2015.12.010.
- Choi AM, Ryter SW, Levine B. Autophagy in human health and disease. N Engl J Med. 2013;368:651–662. doi:10.1056/NEJMra1205406
- Kwanten, WJ, Martinet, W, Francque, SM (2016). Chapter: Authophagy in non-alcoholic fatty liver disease (NAFLD). Intech 455-483. Book: Autophagy in Current Trends in Cellular Physiology and Pathology. Edited by Nikolai V. Gorbunov and Marion Schneider. doi: 10.5772/64534. http://dx.doi.org/10.5772/64534
- Primassin S, Tucci S, Spiekerkoetter U. Hepatic and muscular effects of different dietary fat content in VLCAD deficient mice. Mol Genet Metab. 2011 Dec;104(4):546-51. doi: 10.1016/j.ymgme.2011.09.011.
- Vecchione G, Grasselli E, Cioffi F, Baldini F, Oliveira PJ, Sardão VA, Cortese K, Lanni A, Voci A, Portincasa P, Vergani L. The Nutraceutic Silybin Counteracts Excess Lipid Accumulation and Ongoing Oxidative Stress in an In Vitro Model of Non-Alcoholic Fatty Liver Disease Progression. Front Nutr. 2017 Sep 19;4:42. doi: 10.3389/fnut.2017.00042.
- Baffy G. Uncoupling protein-2 and non-alcoholic fatty liver disease. Front Biosci 2005;10:2082-2096. doi: 10.2741/1683
- Criollo A, Chereau F, Malik SA, Niso-Santano M, Mariño G, Galluzzi L, Maiuri MC, Baud V, Kroemer G. Autophagy is required for the activation of NFκB. Cell Cycle. 2012 Jan 1;11(1):194-9. doi: 10.4161/cc.11.1.18669.
- Schlottmann S, Buback F, Stahl B, Meierhenrich R, Walter P, Georgieff M, Senftleben U. Prolonged classical NF-kappaB activation prevents autophagy upon E. coli stimulation in vitro: a potential resolving mechanism of inflammation. Mediators Inflamm. 2008;2008:725854. doi: 10.1155/2008/725854.
- Ambros V. The functions of animal microRNAs. Nature. 2004 Sep 16;431(7006):350-5. Review. doi:10.1038/nature02871
- Cheung O, Puri P, Eicken C, Contos MJ, Mirashahi F, Maher JW, Kellum JM, Min H, Luketic VA, Sanyal AJ. Nonalcoholic steatohepatitis is associated with altered hepatic microRNA expression. *Hepatology*. 2008;48(6):1810–1820. doi: 10.1002/hep.22569.

- Kong L, Zhu J, Han W, Jiang X, Xu M, Zhao Y, Dong Q, Pang Z, Guan Q, Gao L, Zhao J, Zhao L. Significance of serum microRNAs in pre-diabetes and newly diagnosed type 2 diabetes: a clinical study. Acta Diabetol. 2011 Mar;48(1):61-9. doi: 10.1007/s00592-010-0226-0.
- Jin JC, Zhang X, Jin XL, Quian CS, Jjang H, Ruan Y. MicroRNA-122 regulation of the morphology and cytoarchitecture of hepatoma carcinoma cells. Mol Med Rep. 2014 Apr;9(4):1376-80. doi: 10.3892/mmr.2014.1930.
- Bernardino RL, Marinelli RA, Maggio A, Gena P, Cataldo I, Alves MG, Svelto M, Oliveira PF, Calamita G. Hepatocyte and Sertoli Cell Aquaporins, Recent Advances and Research Trends. Int J Mol Sci. 2016 Jul 9;17(7). pii: E1096. doi: 10.3390/ijms17071096.
- Tesse A, Grossini E, Tamma G, Brenner C, Portincasa P, Marinelli RA, Calamita G. Aquaporins as Targets of Dietary Bioactive Phytocompounds. Front Mol Biosci. 2018 Apr 18;5:30. doi: 10.3389/fmolb.2018.00030.
- Calamita, G, Gena P, Ferri D, Rosito A, Rojek A, Nielsen S, Marinelli RA, Frühbeck G, Svelto M. Biophysical assessment of aquaporin-9 as principal facilitative pathway in mouse liver import of glucogenetic glycerol. Biol Cell. 2012 Jun;104(6):342-51. doi: 10.1111/boc.201100061.
- Jelen, S, Wacker S, Aponte-Santamaría C, Skott M, Rojek A, Johanson U, Kjellbom P, Nielsen S, de Groot BL, Rützler M. Aquaporin-9 protein is the primary route of hepatocyte glycerol uptake for glycerol gluconeogenesis in mice. J Biol Chem. 2011 Dec 30;286(52):44319-25. doi: 10.1074/jbc.M111.297002.
- Calamita G, Delporte C, Marinelli RA (2015). Hepatobiliary, salivary glands and pancreas aquaporins in health and disease In: G. Soveral, A. Casini and S. Nielsen Ed. Int Immunopharmacol.Aquaporins in health and disease: new molecular targets for drug discovery. CRC Press Taylor & Francis Group, ISBN: 9781498707831; Cat# K24910. Chapter 9, pages 183-205.
- Gena P, Buono ND, D'Abbicco M, Mastrodonato M, Berardi M, Svelto M, Lopez L, Calamita G. Dynamical modeling of liver Aquaporin-9 expression and glycerol permeability in hepatic glucose metabolism. Eur J Cell Biol. 2017 Jan;96(1):61-69. doi: 10.1016/j.ejcb.2016.12.003.
- Portincasa P, Palasciano G, Svelto M, Calamita G (2008). Aquaporins in the hepatobiliary tract. which, where, what they do in health and disease. Eur J Clin Invest, 38(1):1-10. doi: 10.1111/j.1365-2362-2007.01897.x.
- Rodríguez A1, Catalán V, Gómez-Ambrosi J, García-Navarro S, Rotellar F, Valentí V, Silva C, Gil MJ, Salvador J, Burrell MA, Calamita G, Malagón MM, Frühbeck G. Insulin- and leptin-mediated control of aquaglyceroporins in human adipocytes and hepatocytes is mediated via the

PI3K/Akt/mTOR signaling cascade. J Clin Endocrinol Metab. 2011 Apr;96(4):E586-97. doi: 10.1210/jc.2010-1408.

- Gena P, Mastrodonato M, Portincasa P, Fanelli E, Mentino D, Rodríguez A, Marinelli RA, Brenner C, Frühbeck G, Svelto M, Calamita G. Liver glycerol permeability and aquaporin-9 are dysregulated in a murine model of Non-Alcoholic Fatty Liver Disease. PLoS One. 2013 Oct 30;8(10):e78139. doi: 10.1371/journal.pone.0078139.
- Rodríguez A, Gena P, Méndez-Giménez L, Rosito A, Valentí V, Rotellar F, Sola I, Moncada R, Silva C, Svelto M, Salvador J, Calamita G, Frühbeck G. Reduced hepatic aquaporin-9 and glycerol permeability are related to insulin resistance in non-alcoholic fatty liver disease. Int J Obes (Lond). 2014 Sep;38(9):1213-20. doi: 10.1038/ijo.2013.234.
- Rodríguez A, Moreno NR, Balaguer I, Méndez-Giménez L, Becerril S, Catalán V, Gómez-Ambrosi J, Portincasa P, Calamita G, Soveral G, Malagón MM, Frühbeck G. Leptin administration restores the altered adipose and hepatic expression of aquaglyceroporins i mproving the non-alcoholic fatty liver of ob/ob mice. Sci Rep. 2015a Jul 10;5:12067. doi: 10.1038/srep12067.
- Rodríguez A, Marinelli RA, Tesse A, Frühbeck G, Calamita G. Sexual Dimorphism of Adipose and Hepatic Aquaglyceroporins in Health and Metabolic Disord ers. Front Endocrinol (Lausanne). 2015b Nov 5;6:171. doi: 10.3389/fendo.2015.00171.
- Cai C, Wang C, Ji W, Liu B, Kang Y, Hu Z, Jiang Z. Knockdown of hepatic aquaglyceroporin-9 alleviates high fat diet-induced non-alcoholic fatty liver disease in rats. 2013 Mar;15(3):550-6. doi: 10.1016/j.intimp.2013.01.020.
- Calamita G and Portincasa P. Present and future therapeutic strategies in non-alcoholic fatty liver disease. Expert Opin Ther Targets. 2007 Sep;11(9):1231-49. doi:10.1517/14728222.11.9.1231
- Calamita G, Perret J, Delporte C. Aquaglyceroporins: Drug Targets for Metabolic Diseases? Front Physiol. 2018 Jul 10;9:851. doi: 10.3389/fphys.2018.00851.
- Molina-Molina E, Lunardi Baccetto R, Wang DQ, de Bari O, Krawczyk M, Portincasa P. Exercising the hepatobiliary-gut axis. The impact of physical activity performance. Eur J Clin Invest. 2018 Aug;48(8):e12958. doi: 10.1111/eci.12958.
- Loguercio C, Festi D. Silybin and the liver: from basic research to clinical practice. World J Gastroenterol. 2011 May 14;17(18):2288-301. doi: 10.3748/wjg.v17.i18.2288.
- Loguercio C, Andreone P, Brisc C, Brisc MC, Bugianesi E, Chiaramonte M, Cursaro C, Danila M, de Sio I, Floreani A, Freni MA, Grieco A, Groppo M, Lazzari R, Lobello S, Lorefice E, Margotti M, Miele L, Milani S, Okolicsanyi L, Palasciano G, Portincasa P, Saltarelli P, Smedile A, Somalvico F, Spadaro A, Sporea I, Sorrentino P, Vecchione

R, Tuccillo C, Del Vecchio Blanco C, Federico A. Silybin combined with phosphatidylcholine and vitamin E in patients with nonalcoholic fatty liv er disease: a randomized controlled trial. Free Radic Biol Med. 2012 May 1;52(9):1658-65. doi: 10.1016/j.freeradbiomed.2012.02.008.

- Clayton DF, Weiss M, Darnell JE, Jr. Liver-specific RNA metabolism in hepatoma cells: variations in transcription rates and mRNA levels. Mol Cell Biol 1985;5:2633-2641.
- Vergani L, Vecchione G, Baldini F, Grasselli E, Voci A, Portincasa P, Ferrari PF, Aliakbarian B, Casazza AA, Perego P. Polyphenolic extract attenuates fatty acid-induced steatosis and oxidative stress in hepatic and endothelial cells. Eur J Nutr. 2018 Aug;57(5):1793-1805. doi: 10.1007/s00394-017-1464-5.
- Zhang W, Kudo H, Kawai K, Fujisaka S, Usui I, Sugiyama T, Tsukada K, Chen N, Takahara T. Tumor necrosis factor-alpha accelerates apoptosis of steatotic hepatocytes from a murine model of non-alcoholic fatty liver disease. Biochem Biophys Res Commun. 2010 Jan 22;391(4):1731-6. doi: 10.1016/j.bbrc.2009.12.144.
- Vecchione G, Grasselli E, Voci A, Baldini F, Grattagliano I, Wang DQ, Portincasa P, Vergani L. Silybin counteracts lipid excess and oxidative stress in cultured steatotic hepatic cells. World J Gastroenterol 2016; 22: 6016-6026. doi: 10.3748/wjg.v22.i26.6016
- Koopman R, Schaart G, Hesselink MK. Optimisation of oil red O staining permits combination with immunofluorescence and automated quantification of lipids. Histochem Cell Biol. 2001 Jul;116(1):63-8.
- Khalil M, Khalifeh H, Baldini F, Salis A, Damonte G, Daher A, Voci A, Vergani L. Antisteatotic and antioxidant activities of Thymbra spicata L. extracts in hepatic and endothelial cells as in vitro models of non-alcoholic fatty liver disease. J Ethnopharmacol. 2019 Jul 15;239:111919. doi: 10.1016/j.jep.2019.111919.
- Atshaves BP, Storey SM, McIntosh AL, Petrescu AD, Lyuksyutova OI, Greenberg AS, Schroeder F. Sterol carrier protein-2 expression modulates protein and lipid composition of lipid droplets. J Biol Chem 2001;276:25324-25335. doi:10.1074/jbc.M100560200
- Folch J, Less M, Sloane Stanely GH. A simple method for the isolation and purification of total lipides from animal tissues. J Biol Chem 1957;226:497-509.
- Grasselli E, Voci A, Canesi L, Salis A, Damonte G, Compalati AD, Goglia F, Gallo G, Vergani L. 3,5-diiodo-L-thyronine modifies the lipid droplet composition in a model of hepatosteatosis. Cell Physiol Biochem 2014; 33: 344-356 PMID: 24525903 doi: 10.1159/000356674.
- Morrison WR and Smith LM. Preparation of fatty acid methyl esters and dimethylacetals from lipids with boron fluoride. J Lipid Res 1964;5:600-608.

- Grasselli E, Voci A, Demori I, Vecchione G, Compalati AD, Gallo G, Goglia F, De Matteis R, Silvestri E, Vergani L. Triglyceride Mobilization from Lipid Droplets Sustains the Anti-Steatotic Action of Iodothyronines in Cultured Rat Hepatocytes. Front Physiol. 2016 Jan 12;6:418. doi: 10.3389/fphys.2015.00418.
- Vecchione G, Grasselli E, Compalati AD, Ragazzoni M, Cortese K, Gallo G, Voci A, Vergani L. Ethanol and fatty acids impair lipid homeostasis in an in vitro model of hepatic steatosis. Food Chem Toxicol. 2016 Apr;90:84-94. doi: 10.1016/j.fct.2016.02.004. Epub 2016 Feb 5.
- Baselga-Escudero L, Pascual-Serrano A, Ribas-Latre A, Casanova E, Salvadó MJ, Arola L, Arola-Arnal A, Bladé C. Long-term supplementation with a low dose of proanthocyanidins normalized liver miR-33a and miR-122 levels in high-fat diet-induced obese rats. Nutr Res. 2015 Apr;35(4):337-45. doi: 10.1016/j.nutres.2015.02.008.
- Moyes CD, Mathieu-Costello OA, Tsuchiya N, Filbur C, Hansford RG. Mitochondrial biogenesis during cellular differentiation. Am. J. Physiol. 272 (1997) Cl345-Cl351. doi:10.1152/ajpcell.1997.272.4.C1345
- LaemmLi UK. Cleavage of structural proteins during the assembly of the head of bacteriophage T4. Nature. 1970 Aug 15;227(5259):680-5. doi:10.1038/227680a0
- Towbin H, Staehelin T, Gordon J. Electrophoretic transfer of proteins from polyacrylamide gels to nitrocellulose sheets: procedure and some applications. Proc Natl Acad Sci U S A. 1979 Sep;76(9):4350-4. doi:10.1073/pnas.76.9.4350
- Tanida I, Ueno T, Kominami E. LC3 conjugation system in mammalian autophagy. Int J Biochem Cell Biol. 2004 Dec;36(12):2503-18. doi:10.1016/j.biocel.2004.05.009
- Tsai WC, Hsu MT, Lai TC, Chau GY, Lin CW, Chen CM, Lin CD, Liao YL, Wang JL, Chau YP, Hsu MT, Hsiao M, Huang HD, Tsou AP. MicroRNA-122, a tumor suppressor microRNA that regulates intrahepatic metastasis of hepatocellular carcinoma. Hepatology. 2009 May;49(5):1571-82. doi: 10.1002/hep.22806.
- Grasselli E, Baldini F, Vecchione G, Oliveira PJ, Sardão VA, Voci A, Portincasa P, Vergani L. Excess fructose and fatty acids trigger a model of non-alcoholic fatty liver disease progression in vitro: Protective effect of the flavonoid silybin. Int J Mol Med. 2019 Aug;44(2):705-712. doi: 10.3892/ijmm.2019.4234.
- Grattagliano I, Diogo CV, Mastrodonato M, de Bari O, Persichella M, Wang DQ, Liquori A, Ferri D, Carratù MR, Oliveira PJ, Portincasa P. A silybin-phospholipids complex counteracts rat fatty liver degeneration and mitochondrial oxidative changes. World J Gastroenterol. 2013 May 28;19(20):3007-17. doi: 10.3748/wjg.v19.i20.3007.

- Cullen JM. Mechanistic classification of liver injury. Toxicol Pathol. 2005;33(1):6-8. doi:10.1080/01926230590522428
- Bacq Y. Acute fatty liver of pregnancy. Semin Perinatol. 1998 Apr;22(2):134-40. doi: 10.1016/s0146-0005(98)80045-1
- Ramachandran R, Kakar S. Histological patterns in drug-induced liver disease. J Clin Pathol. 2009 Jun;62(6):481-92. doi: 10.1136/jcp.2008.058248.
- Horton JD, Cohen JC, Hobbs HH. PCSK9: a convertase that coordinates LDL catabolism. J Lipid Res. 2009 Apr;50 Suppl:S172-7. doi: 10.1194/jlr.R800091-JLR200. Epub 2008 Nov 19.
- Cohen JC, Boerwinkle E, Mosley TH Jr, Hobbs HH. Sequence variations in PCSK9, low LDL, and protection against coronary heart disease. N Engl J Med. 2006 Mar 23;354(12):1264-72. doi:10.1056/NEJMoa054013
- Benn M, Nordestgaard BG, Grande P, Schnohr P, Tybjaerg-Hansen A. PCSK9 R46L, low-density lipoprotein cholesterol levels, and risk of ischemic heart disease: 3 independent studies and meta-analyses. J Am Coll Cardiol. 2010 Jun 22;55(25):2833-42. doi: 10.1016/j.jacc.2010.02.044.
- Dubuc G, Chamberland A, Wassef H, Davignon J, Seidah NG, Bernier L, Prat A. Statins upregulate PCSK9, the gene encoding the proprotein convertase neural apoptosis-regulated convertase-1 implicated in familial hypercholesterolemia. Arterioscler Thromb Vasc Biol. 2004 Aug;24(8):1454-9. Epub 2004 Jun 3. doi:10.1161/01.ATV.0000134621.14315.43
- Huijgen R, Boekholdt SM, Arsenault BJ, Bao W, Davaine JM, Tabet F, Petrides F, Rye KA, DeMicco DA, Barter PJ, Kastelein JJ, Lambert G. Plasma PCSK9 levels and clinical outcomes in the TNT (Treating to New Targets) trial. J Am Coll Cardiol. 2012 May 15;59(20):1778-84. doi: 10.1016/j.jacc.2011.12.043.
- Skottová N, Krecman V. Silymarin as a potential hypocholesterolaemic drug. Physiol Res. 1998;47(1):1-7.
- Cicero, A.F.G.; Colletti, A.; Bajraktari, G.; Descamps, O.; Djuric, D.M.; Ezhov, M.; Fras, Z.; Katsiki, N.; Langlois, M.; Latkovskis, G., et al. Lipid-lowering nutraceuticals in clinical practice: position paper from an International Lipid Expert Panel. Nutrition reviews 2017, 75, 731-767. doi:10.1093/nutrit/nux047.
- Voroneanu L, Nistor I, Dumea R, Apetrii M, Covic A. Silymarin in Type 2 Diabetes Mellitus: A Systematic Review and Meta-Analysis of Randomized Controlled Trials. J Diabetes Res. 2016;2016:5147468. doi: 10.1155/2016/5147468.

- Lindskog C, Asplund A, Catrina A, Nielsen S, Rützler M. A Systematic Characterization of Aquaporin-9 Expression in Human Normal and Pathological Tissues. J Histochem Cytochem. 2016 May;64(5):287-300. doi: 10.1369/0022155416641028.
- Joven, J, Micol, V, Segura-Carretero, A, Alonso-Villaverde, C, Menéndez, JA (2014). Bioactive food components platform. Crit Rev Food Sci Nutr 54(8):985-100. doi: 10.1080/10408398.2011.621772
- Komatsu M, Waguri S, Ueno T, Iwata J, Murata S, Tanida I, Ezaki J, Mizushima N, Ohsumi Y, Uchiyama Y, Kominami E, Tanaka K, Chiba T. Impairment of starvation-induced and constitutive autophagy in Atg7-deficient mice. J Cell Biol 2005;169:425-34 PMID: 15866887 doi: 10.1083/jcb.200412022.
- Trocoli A, Djavaheri-Mergny M. The complex interplay between autophagy and NF-κB signaling pathways in cancer cells. Am J Cancer Res. 2011;1(5):629-49.
- Ravikumar B1, Sarkar S, Davies JE, Futter M, Garcia-Arencibia M, Green-Thompson ZW, Jimenez-Sanchez M, Korolchuk VI, Lichtenberg M, Luo S, Massey DC, Menzies FM, Moreau K, Narayanan U, Renna M, Siddiqi FH, Underwood BR, Winslow AR, Rubinsztein DC. Regulation of mammalian autophagy in physiology and pathophysiology. Physiol Rev. 2010 Oct;90(4):1383-435. doi: 10.1152/physrev.00030.2009.
- Rubinsztein DC, Codogno P, Levine B. Autophagy modulation as a potential therapeutic target for diverse diseases. Nat Rev Drug Discov. 2012 Sep;11(9):709-30. doi: 10.1038/nrd3802
- Wacker SJ, Aponte-Santamaría C, Kjellbom P, Nielsen S, de Groot BL, Rützler M. The identification of novel, high affinity AQP9 inhibitors in an intracellular binding site. Mol Membr Biol. 2013 May;30(3):246-60. doi: 10.3109/09687688.2013.773095.
- Sonntag Y, Gena P, Maggio A, Singh T, Artner I, Oklinski MK, Johanson U, Kjellbom P, Nieland JD, Nielsen S, Calamita G, Rützler M. Identification and characterization of potent and selective aquaporin-3 and aquaporin-7 inhibitors. J Biol Chem. 2019 May 3;294(18):7377-7387. doi: 10.1074/jbc.RA118.006083.

Table 1. Characteristics of the primer pairs used for the RT-qPCR analysis.

Primer name	Primer sequence (5’ -> 3’)	Annealing temperature (°C)	Accession ID
GAPDH-Fw	GACCCCTTCATTGACCTCAAC	60	DQ403053
GAPDH-Rv	CGCTCCTGGAAGATGGTGATGGG		
ATG7-Fw	CCTCAGCGGATGTATGGACC	60	NM_001012097.1
ATG7-Rv	AGCCACATTACACCCCAAGG		
AQP9- Fw	CGTAGGAGAAAATGCAACAGC	60	NM_022960
AQP9-Rv	TGGCAAAGACGATCAGAAGG		
SCD-1 Fw	CACACGCCGACCCTCACAACT	60	AF509569
SCD-1 Rv	TCCGCCCTTCTCTTTGACAGCC		
PCSK9 Fw	GCTTCAGCGGCTTGTTCCT	60	NC_005104.4
PCSK9 Rv	TGCTCCTCCACTCTCCACATAA		
VLCAD Fw	TGAATGACCCTGCCAAG	60	NM 012891
VLCAD Rv	CCACAATCTCTGCCAAGC		
UCP2 Fw	CGTCGGACCTAGCCGTCTGCA	56	BC062230
UCP2 Rv	CGGAGTCGGGAGGGTGCTTTG		

FIGURE LEGENDS

Figure 1. Effect of silybin on fatty acid accumulation.

FaO cells were incubated in the presence of oleate/palmitate (SS), or oleate/palmitate and TNFα (SH), then treated for 24 h with 50 μM silybin (Sil). Untreated FaO cells were used as control (Ctrl). **A.** Representative micrographs of FaO cells stained with DAPI and Oil-Red-O (ORO) (magnification 40x). **B-C.** Average size of LDs and number of LDs/cells. Values are mean±S.D. from at least three independent experiments. Statistical significance between groups was assessed by ANOVA followed by Tukey's test. Symbols: Ctrl *vs*. all treatments *p≤0.001; SS *vs*. all treatments & p≤0.001.

Figure 2. Effect of silybin on fatty acids composition of LDs.

FaO cells were incubated in presence of oleate/palmitate (SS), or oleate/palmitate and TNFα (SH), then treated for 24 h with 50 μM silybin (Sil). Untreated FaO cells were used as control (Ctrl). **A.** Acyl composition of LDs purified and analyzed by gas chromatography. **B.** Real-time qPCR analysis of SCD-1 transcriptional expression. Values are mean±S.D. from at least three independent experiments. Statistical significance between groups was assessed by ANOVA followed by Tukey's test. Symbols: Ctrl *vs*. all treatments *p≤0.05, **p≤0.01, ***p≤0.001; SS *vs*. all treatments &p≤0.05, &&&p≤0.001; SH *vs*. all treatments # p≤0.05.

Figure 3. Effect of silybin on AQP9 expression and glycerol import.

FaO cells were incubated with oleate/palmitate (SS), or oleate/palmitate and TNFα (SH), then treated for 24 h with 50 μM silybin (Sil). Untreated FaO cells were used as control (Ctrl). **A.** Real-time qPCR analysis of *AQP9* transcriptional expression. **B-F**. Immunofluorescence analysis. AQP9 immunoreactivity (*green fluorescence*) is seen over the plasma membrane. Nuclei are stained by DAPI (*blue fluorescence*). **G**. Glycerol content of culture medium. Values are mean±S.D. from at least three independent experiments. Statistical significance between groups was assessed by ANOVA followed by Tukey's test. Symbols: Ctrl *vs*. all treatments ***p≤0.001; SS *vs*. all treatments &&p≤0.01, &&&p≤0.001; SH *vs*. all treatments ### p≤0.001).

Figure 4. Effect of silybin on hepatocyte autophagy.

A-E. Immunofluorescence analysis. LC3-II immunoreactivity (*green fluorescence*) is seen over the plasma membrane. Nuclei are stained by DAPI (*blue fluorescence*). Control cells **(A)** show few punctuate structures (*green dots*) indicating LC3 recruitment on autophagosomes. Both SS **(B)** and

SH **(D)** hepatocytes show an increase in these cytosolic puncta reflecting an increase in autophagy turnover. The immunofluorescence becomes more diffuse in SS and SH cells were treated with silybin **(C, E)**, resulting in a pattern more similar to that of control cells. **F.** Western blot analysis of LC3-II/LC3-I ratio. Both SS and SH cells show a significant increase in LC3-II/LC3-I ratio, while silybin counteracts this increase in both steatotic conditions. **G.** Real-time qPCR analysis of *Atg7* transcriptional expression. In both steatotic conditions, Atg7 mRNA results overexpressed, largely in SH cells compared to SS cells. The treatment with silybin restores the Atg7 expression near to control in SH hepatocytes. **H.** Western blot analysis of NF-κB. A significant decrease in NF-κB activation is observed when both SS and SH hepatocytes are treated with silybin. Values are mean±S.D. from at least three independent experiments. Statistical significance between groups was assessed by ANOVA followed by Tukey's test. Symbols: Ctrl *vs*. all treatments *p≤0.05, ***p≤0.001; SS *vs*. all treatments &&&p≤0.001, SH *vs*. all treatments ###p≤0.001.

Figure 5. Effects of silybin on genes of hepatic lipid metabolism.

FaO cells were incubated in the presence of oleate/palmitate (SS), or oleate/palmitate and TNFα (SH), then treated for 24 h with 50 μM silybin (Sil). Untreated FaO cells were used as control (Ctrl). **A.** Real-time qPCR analysis of *PCSK9* transcriptional expression. **B.** Real-time qPCR analysis of VLCAD transcriptional expression. **C.** Cytochrome C oxidase activity measured by enzymatic assay. **D.** Real-time qPCR analysis of UCP2 transcriptional expression. **E.** Real-time qPCR analysis of miR-122 transcriptional expression. The level of miR-122 is increased in SS cells upon treatment with silybin. Values are mean±S.D. from at least three independent experiments. Statistical significance between groups was assessed by ANOVA followed by Tukey's test. Symbols: Ctrl *vs*. all treatments ** p≤0.01, ***p≤0.001; SS *vs*. all treatments &&&p≤0.001; SH *vs*. all treatments ###p≤0.001.).

A

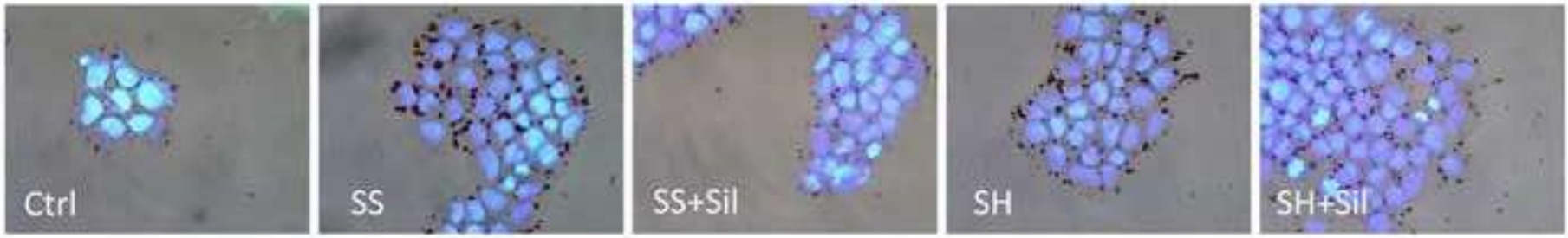

B

LDs number / cell

	Ctrl	SS	SS+Sil	SH	SH+Sil
Mean	72	294 *	248 *	296 *	328 *
Std. Deviation	1.41	161	24	58.7	9.19

* p≤0.001 vs Ctrl

C

LD diameter (µm)

	Ctrl	SS	SS+Sil	SH	SH+Sil
Mean	0.93	1.49	1.11 #	1.33 #	1.22 #
Std. Deviation	0.60	1.38	1.12	1.47	1.22

p≤0.001 vs SS

A

	SS	SS+Sil	SH	SH+Sil
SFA/UFA	5.66	7.56	13.63	6.98
<C16 (%)	11.59	15.88	4.29	18.56

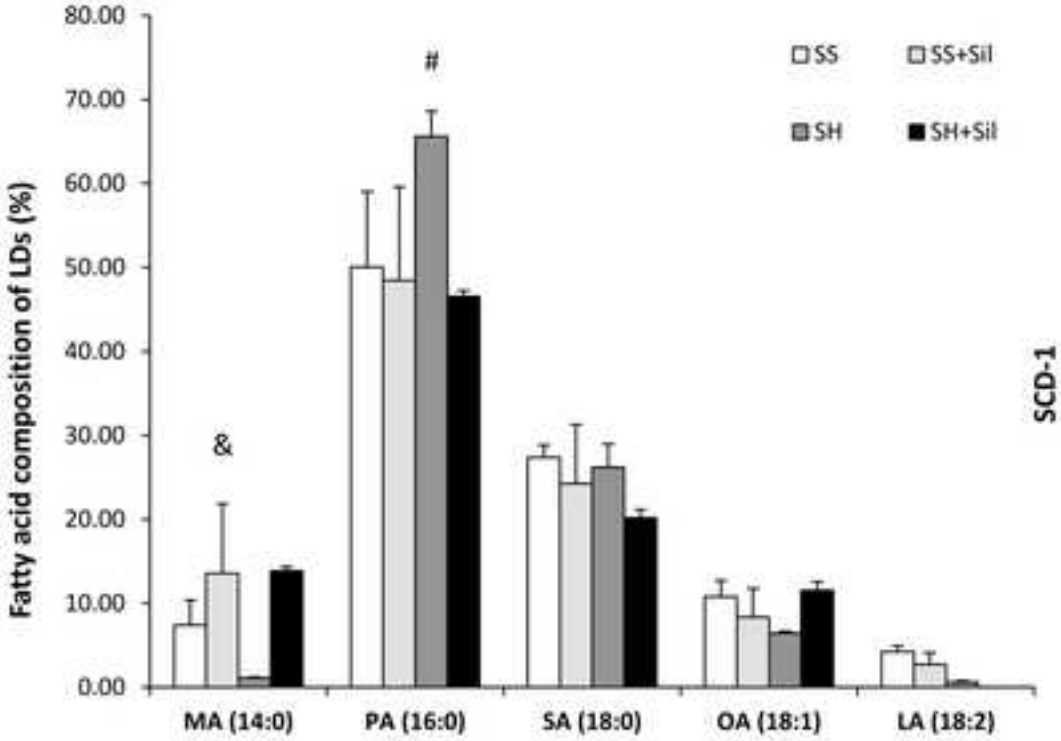

B

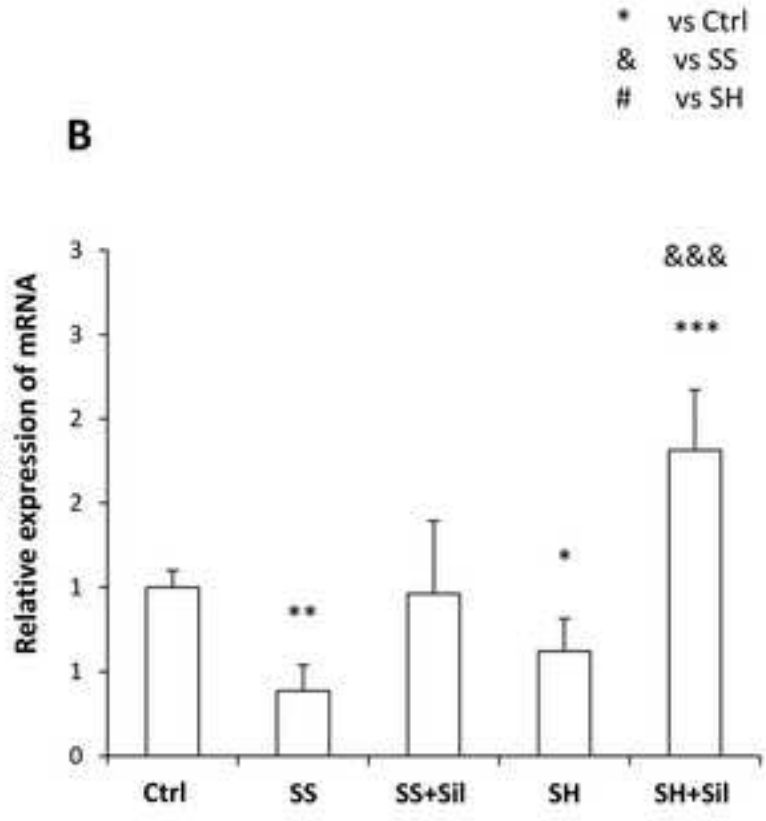

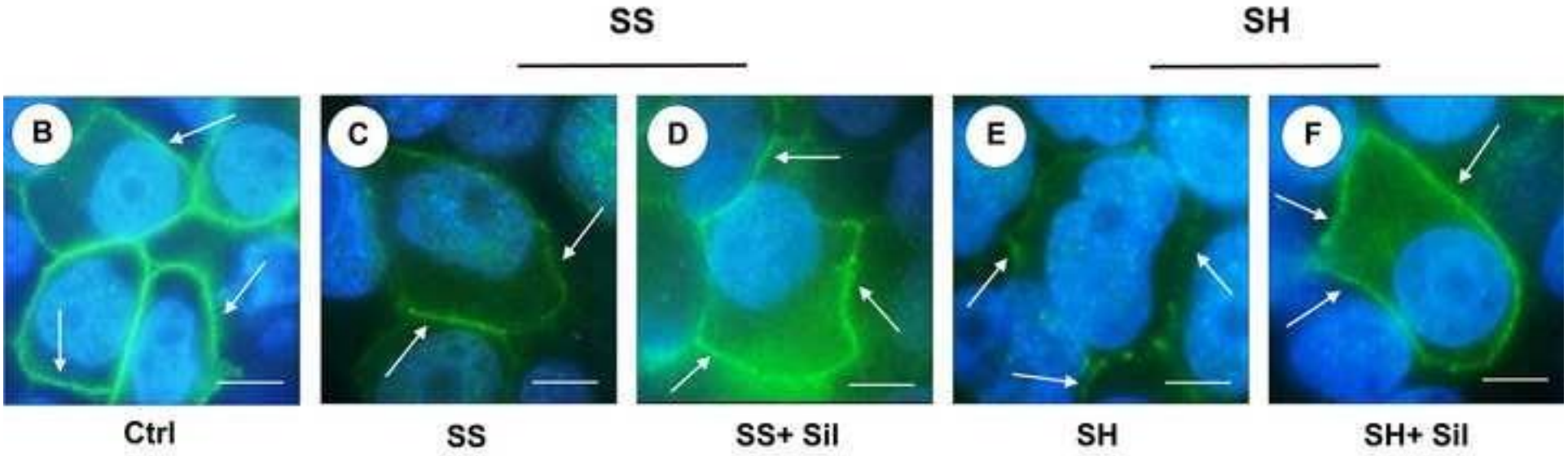
SS
SH
B
C
D
E
F
Ctrl
SS
SS+ Sil
SH
SH+ Sil

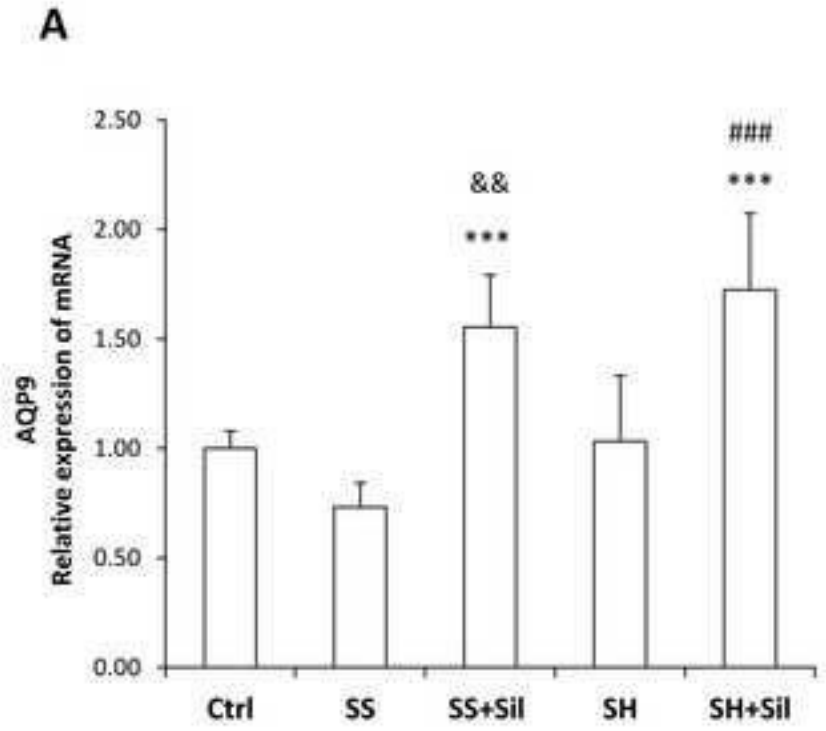
A
AQP9
Relative expression of mRNA
2.50
2.00
1.50
1.00
0.50
0.00
&&
***
###
***
Ctrl
SS
SS+Sil
SH
SH+Sil

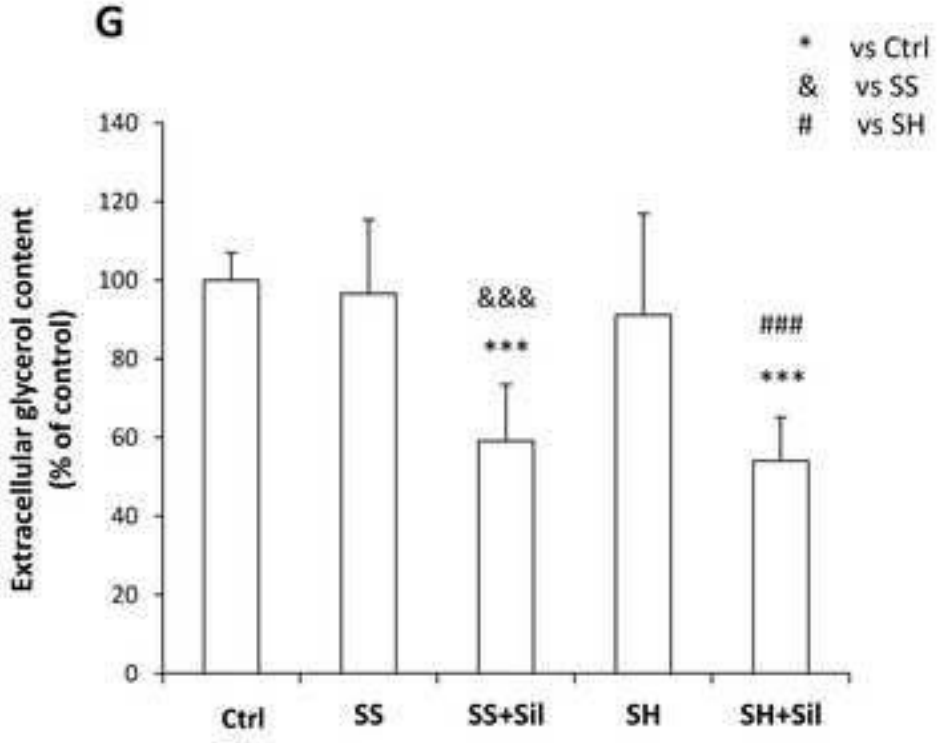
G
* vs Ctrl
& vs SS
# vs SH
Extracellular glycerol content
(% of control)
140
120
100
80
60
40
20
0
&&&
***
###
***
Ctrl
SS
SS+Sil
SH
SH+Sil

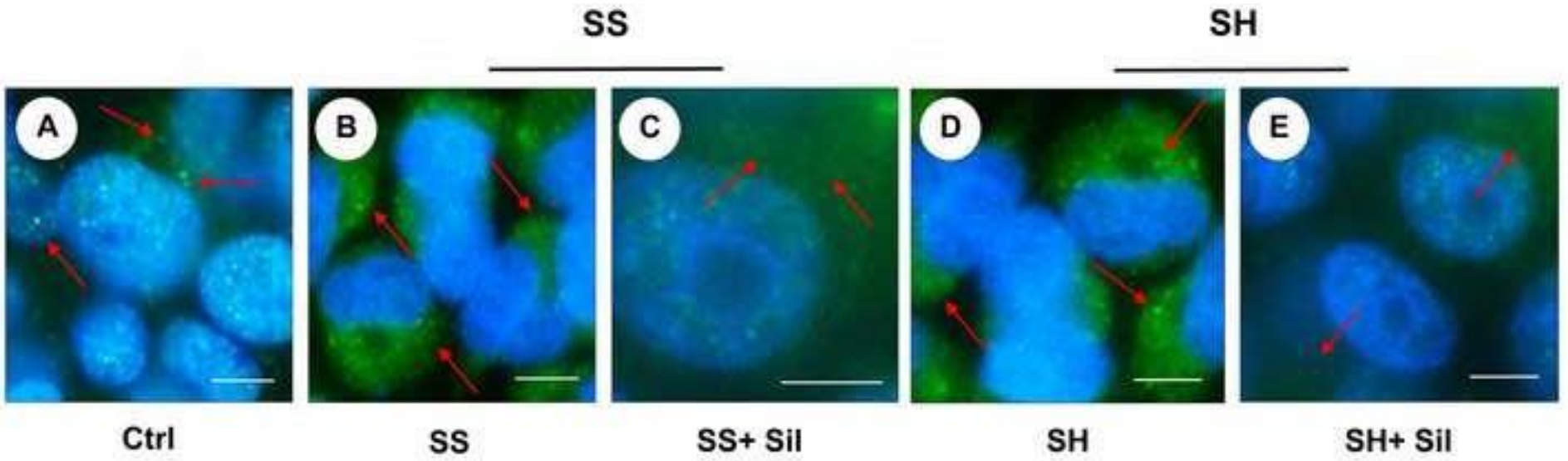
SS
SH
A
B
C
D
E
Ctrl
SS
SS+ Sil
SH
SH+ Sil

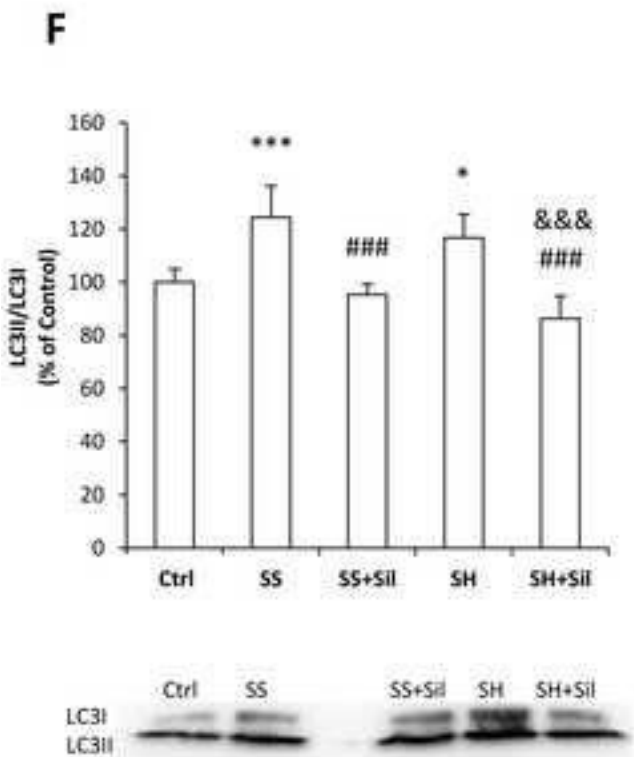
F
LC3II/LC3I (% of Control)
160
140
120
100
80
60
40
20
0
***
*
###
###
&&&
Ctrl
SS
SS+Sil
SH
SH+Sil
Ctrl
SS
SS+Sil
SH
SH+Sil
LC3I
LC3II

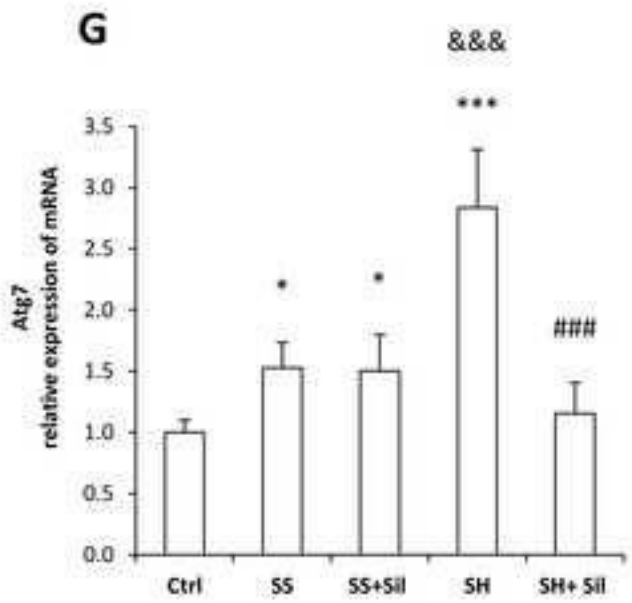
G
Atg7 relative expression of mRNA
3.5
3.0
2.5
2.0
1.5
1.0
0.5
0.0
&&&
***
*
*
###
Ctrl
SS
SS+Sil
SH
SH+ Sil

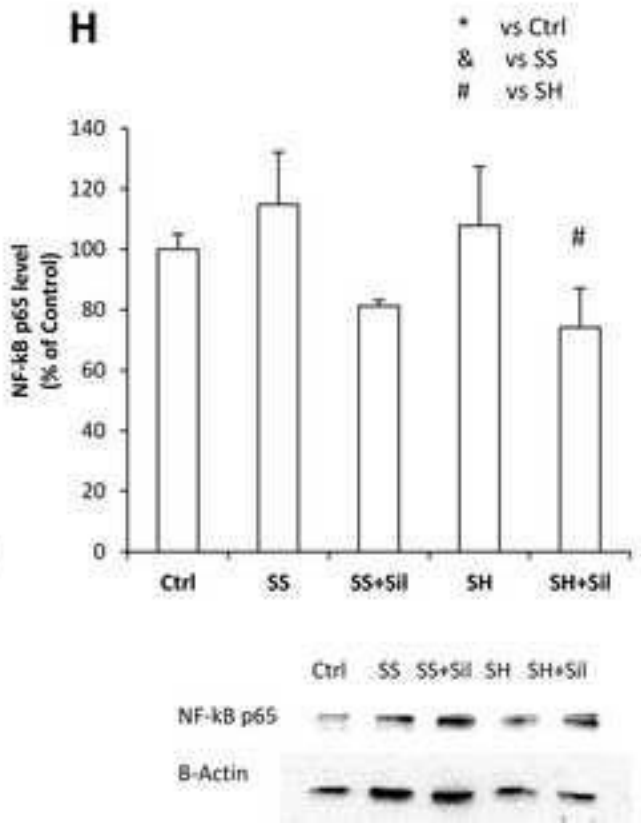
H
* vs Ctrl
& vs SS
# vs SH
NF-kB p65 level (% of Control)
140
120
100
80
60
40
20
0
#
Ctrl
SS
SS+Sil
SH
SH+Sil
Ctrl
SS
SS+Sil
SH
SH+Sil
NF-kB p65
B-Actin